Magnetic structure, magnetization, and magnetotransport properties of $(Ba,Sr)M_{2\pm x}T_{4\mp x}O_{11}$ (M=Fe,Co; T=Ru,Ti)

L. Shlyk,[1,*] B. G. Ueland,[2] J. W. Lynn,[2] Q. Huang,[2] L. E. De Long,[1] and S. Parkin[3]
[1]*Department of Physics and Astronomy, University of Kentucky, Lexington, Kentucky 40506-0055, USA*
[2]*NIST Center for Neutron Research, National Institute of Standards and Technology, Gaithersburg, Maryland 20899, USA*
[3]*Department of Chemistry, University of Kentucky, Lexington, Kentucky 40506-0055, USA*
(Received 3 March 2010; revised manuscript received 9 April 2010; published 17 May 2010)

Hexagonal R-type ferrites $(Ba,Sr)M_{2\pm x}T_{4\mp x}O_{11}$ (M=Fe,Co; T=Ru,Ti) were studied via neutron and x-ray diffraction, magnetization, and electrical transport measurements. Magnetization data for single-crystal $BaFe_{3.26}Ti_{2.74}O_{11}$ reveal two magnetic transitions at T_1=250 K and T_2=84 K, which indicates complex magnetic order driven by competing interactions on a frustrated lattice with a noncentrosymmetric structure. Magnetization data for single-crystal $BaCo_{1.85}Ru_{4.15}O_{11}$ reveal soft ferromagnetic order at T_C=105 K with an easy direction perpendicular to the **c** axis. Neutron diffraction data for polycrystalline $BaCo_{1.68}Ru_{4.32}O_{11}$ indicate a nearly compensated arrangement of spins lying within the **a**-**b** plane with a possible canting out of the plane that yields nonzero scalar spin chirality. The transverse magnetoresistivity ρ_{xy} of single-crystal $BaCo_{1.85}Ru_{4.15}O_{11}$ for current $\boldsymbol{J}\|\boldsymbol{H}\perp\mathbf{c}$ axis is typical of an anomalous Hall effect observed in ferromagnets, whereas for $\boldsymbol{J}\perp\boldsymbol{H}\|\mathbf{c}$ axis, ρ_{xy} is a nonmonotonic function of the magnetic field, consistent with a topological Hall effect that depends upon scalar spin chirality. Neutron diffraction reveals transitions to ferrimagnetic order at T_C=262(1) K for single-crystal $SrFe_{2.6}Ru_{3.4}O_{11}$, and at T_C=403 K for polycrystalline $SrFe_{2.96}Ru_{3.04}O_{11}$ (refined as a collinear structure at T=5 K).

DOI: 10.1103/PhysRevB.81.184415 PACS number(s): 75.50.Gg, 75.25.−j, 75.47.Lx

I. INTRODUCTION

The discovery of materials can lead to observations of unexpected physical properties that subsequently underpin innovative technologies, as well as extend our fundamental understanding of condensed matter physics. In particular, there is an ongoing quest for new materials for spin-transport electronics (spintronics), in which the spin of charge carriers is exploited to provide enhanced functionalities for submicron device structures[1,2] such as spin-based field effect transistors, spin-based light emitting diodes, and nonvolatile memory.[3,4] This has stimulated an intensive effort to discover room-temperature ferromagnetic (FM) semiconductors (FS) that are compatible with narrow-gap semiconducting materials commonly employed in current device structures. However, bulk FS that maintain robust magnetic properties at room temperature have proven to be extremely rare. Materials such as half-metallic CrO_2 or Fe_3O_4 support high Curie temperatures, but their complex thermodynamically driven properties have so far inhibited device fabrication.[5–8] Dilute magnetic semiconductors (DMSs), such as (Ga,Mn)As and (Zn,Co)O, have been the most intensively studied prospects for spintronic devices. However, these materials suffer from large gradients of magnetization and electrical conductivity due to the clustering of magnetic dopants within the semiconductor host.[9,10] Therefore, it is crucial to discover alternative FS and understand the fundamental mechanisms that control high-T_C ferromagnetism in semiconductors.

The Fe-bearing R-type ferrites, $(Ba,Sr)Fe_{2\pm x}Ru_{4\mp x}O_{11}$, provide promising candidates for spin-based, multifunctional materials. These compositions exhibit long-range magnetic order below unusually high critical temperatures T_C ~490 K, accompanied by narrow-gap semiconducting properties that include a large anomalous Hall conductance, low resistivity, and high-carrier concentration.[11,12] These characteristics compare quite favorably with the criteria for practical FS. In particular, $BaFe_{3.4}Ru_{2.6}O_{11}$ exhibits a substantial ordered moment ($1.25\mu_B$/f.u.) and a high-Curie temperature (440 K), yet is semiconducting with a small gap (15–20 meV) and nearly ideal coercive field (92 Oe, easy axis) at T=300 K. The room-temperature resistivities of the Ba- and Sr-based Fe ferrites are in the range of typical narrow-gap semiconductors (0.001–100 Ω cm) and therefore can optimize spin injection and detection efficiencies across a doped-semiconductor/FS interface. Moreover, the magnetic ions in R-type ferrites reside within periodic sublattices,[13] in contrast with the random location of magnetic elements in DMS.

The R-type ferrite structure (Fig. 1) can be derived from that of the 6H perovskites since Ba (or Sr) and O form a distorted hexagonal-close-packed motif with Ba (or Sr) located in anti-cuboctahedral coordination by O.[13–15] An occupation of additional oxygen octahedra by Ru and M in the $M(1)$ (4e) and $M(2)$ (6g) sites, and concomitant replacement of Ba(Sr) by O, leads to the so-called "R-type" structure with the general composition quoted for the title compounds. Additionally, trigonal bipyramids (formed by two face-sharing tetrahedra) have voids denoted as $M(3)$ (2d) sites that are exclusively occupied by 3d elements (i.e., Fe, Co), whereas the octahedral voids are occupied by both 4d (Ru) and 3d (Ti, Fe, or Co) elements. The R-type ferrite structure is conveniently viewed as built up from (001) layers of edge-sharing oxygen octahedra surrounding Ru and 3d species located on $M(2)$ sites within a kagome net formed by an ordered array of unoccupied octahedral voids. The kagome layers are connected along [001] via pairs of the face-sharing octahedra centered by $M(1)$ sites, and trigonal bipyramids centered by $M(3)$ sites.

Wide homogeneity ranges are accessible in R-type ferrites via different 4d/3d-transition element compositions that al-

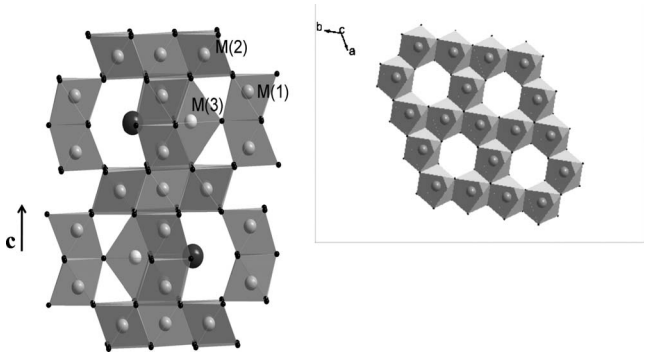

FIG. 1. Left panel: crystal structure of $(Ba,Sr)M_{2\pm x}T_{4\mp x}O_{11}$ (M=Fe,Co, T=Ru,Ti). The $M(1)$ ($4e$) sites are predominantly occupied by Ru, the $M(2)$ ($6g$) sites on the kagome sublattice are occupied by both Ru and appropriate $3d$ elements, and the $M(3)$ ($2d$) sites are predominantly occupied by the appropriate $3d$ elements (Ref. 13). Right panel: arrangement of coordination polyhedra of transition metal ions in the **ab**-(kagome) plane.

low one to engineer desirable electrical transport properties and tune the strength of FM interactions, magnetic anisotropy, and T_C within a single structure type. For example, the high T_C and semiconductivity of Fe-bearing ferrites can be easily tuned by simple substitution of Fe by Co or Mn, which leads to more metallic behavior and much lower T_C's.[11] These variations are apparently due to dramatic changes in electronic or/and magnetic structure induced by rather subtle variations in the chemistry and crystal structure of these systems. Moreover, the hexagonal basal plane lattice parameter changes by less than 0.1% over the known homogeneity ranges, which opens the prospect of fabrication of epitaxially grown thin-film heterostructures composed of R-type ferrite compositions having very different magnetic and electrical properties.

Of particular importance is the linear variation of the Curie temperature with increasing semiconducting gap observed for Fe-bearing R-type ferrites,[11] which differs markedly from the behavior of known DMS, where higher T_c accompanies higher carrier concentration and metallicity. The microscopic origin of this unique trend remains to be resolved, but it provides an important clue concerning the mechanism of high-temperature ferromagnetism in these materials.

The limited disorder generated by mixed occupancy of the $M(2)$ sites by the Ru and M species in the frustrated (**a**-**b**) kagome sublattice of R-type ferrites gives rise to unusual physical properties, including spin chirality[16] and high-T_C ferrimagnetism.[17] $BaMn_2Ru_4O_{11}$ was recently found to exhibit a noncoplanar structure of antiferromagnetically coupled spins ($S>1/2$) with nonzero scalar chirality within a magnetically ordered state.[14] Spin chirality has attracted increasing attention because of its important role in intriguing phenomena such as high-temperature superconductivity[18] and multiferroicity.[19] In addition, spin chirality is predicted to induce a finite Berry phase that acts as a gauge field on the conduction electrons and leads to an "anomalous Hall effect of topological origin."[20–22] The coupling between conduction electrons and a chiral spin structure enhances the magnitude of the topological Hall effect (THE) above that of a conventional AHE expected for a collinear ferromagnet with spin-orbit coupling.[20] Currently, there are few experimental studies of spin chirality in frustrated magnets,[20,23] and little is known about how a nontrivial magnetic structure affects the quantum transport of electrons.

In the following we present the results of combined study of crystal and magnetic structures of selected R-type ferrites and consider the influence of magnetic structure on the electron transport in these materials. In particular, we report x-ray diffraction and magnetic data on a single-crystal ferrite of composition $BaFe_{3.26}Ti_{2.74}O_{11}$, together with neutron scattering results for both single-crystal and polycrystalline $(Ba,Sr)M_{2\pm x}Ru_{4\mp x}O_{11}$ (M=Fe,Co) samples. Despite the magnetic frustration inherent in the R-type structure when antiferromagnetic (AFM) interactions exist on the kagome planes, we observe robust magnetic ground states that are stabilized near and above room temperature via spin canting or collinear alignment along the **c** direction. Moreover, we propose that the anomalous transverse magnetoresistivity of single-crystal $BaCo_{1.85}Ru_{4.15}O_{11}$ is best understood in the context of a THE driven by spin chirality within a magnetically ordered state.

II. EXPERIMENTAL DETAILS

Single crystals of R-type ferrites were grown in a $BaCl_2$ ($SrCl_2$) flux as previously described,[13] and representative x-ray refinements and microprobe analyses have been previously reported.[11–13] Polycrystalline samples of Fe- and Co-bearing ferrites were synthesized by heating stoichiometric mixtures of $BaCO_3$ ($SrCO_3$), RuO_2, and either Fe_2O_3 or Co_3O_4 to 1190 °C for 10 h. X-ray diffraction data for a $BaFe_{3.26}Ti_{2.74}O_{11}$ single crystal were collected at T=90 K using a Nonius Kappa charge-coupled device diffractometer with Mo $K\alpha$ radiation (wavelength λ=0.710 73 Å). Information concerning the data collection and results of the structural refinements for a $BaFe_{3.26}Ti_{2.74}O_{11}$ single crystal are collected in Table I, and Table II gives the determined atomic coordinates and displacement parameters. The magnetizations M of oriented single crystals and polycrystalline samples were measured over a temperature range 5 K$\leq T \leq$300 K in applied magnetic fields 0 T$\leq \mu_o H \leq$5 T using a quantum design MPMS5 magnetometer. The transverse magnetoresistivity ρ_{xy} was measured using the MPMS5 external device control option and a dc four-probe method with currents 5 mA$\leq |J| \leq$20 mA directed in the **ab** plane.

Neutron powder diffraction measurements on polycrystalline $BaCo_{1.68}Ru_{4.32}O_{11}$ and $SrFe_{2.96}Ru_{3.04}O_{11}$ were carried out at the NIST Center for Neutron Research (NCNR) on the BT1 high-resolution powder diffractometer. The (311) reflection of Ge or Cu was used to produce monochromatic neutron beams with wavelengths λ=2.079 and 1.540 Å, respectively. Diffraction measurements were made over an angular range of 2θ=3° to 168° in steps of 0.05°, and 15′, 20′, and 7′ collimators were used on the in pile, monochromatic, and diffracted beams, respectively. The sample was placed in either a V or Al container filled with He exchange gas and mounted in a closed-cycle He refrigerator capable of reach-

TABLE I. Crystal data and structure refinement for single-crystal $BaFe_{3.26}Ti_{2.74}O_{11}$.

Empirical formula	$BaFe_{3.26}Ti_{2.74}O_{11}$
Formula weight	1253.87
Temperature	90.0(2) K
Wavelength	0.71073 A
Crystal system, space group	Hexagonal, P 63/m m c
Unit cell dimensions	a=5.8370(8) Å alpha=90°
	b=5.8370(8) Å beta=90°
	c=13.616(3) Å gamma=120°
Volume	401.77(11) $Å^3$
Z, calculated density	1, 5.182 Mg/m^3
Absorption coefficient	13.211 mm^{-1}
F(000)	578
Crystal size	0.05×0.05×0.02 mm
Theta range for data collection	2.99°–27.37°
Limiting indices	$-7 \le h \le 7$, $-7 \le k \le 7$, $-17 \le l \le 17$
Reflections collected/unique	7898/209 [R(int)=0.0540]
Completeness to theta=27.37	100.0%
Absorption correction	Semiempirical from equivalents
Maximum and minimum transmission	0.778 and 0.558
Refinement method	Full-matrix least-squares on F^2
Data/restraints/parameters	209/0/23
Goodness-of-fit on F^2	1.265
Final R indices [I>2 sigma(I)]	R_1=0.0375, wR_2=0.1040
R indices (all data)	R_1=0.0406, wR_2=0.1070
Largest diffraction peak and hole	4.337 and −5.540 e A^{-3}

ing temperatures from T=10 to 600 K. Data were refined using GSAS (Ref. 24) or the FULLPROF program suite,[25] and magnetic representational analysis was performed using the program SARAH.[26] Detailed measurements of the temperature dependence of the (101) Bragg peak for polycrystalline $BaCo_{1.68}Ru_{4.32}O_{11}$ and the (100) Bragg peaks for polycrystalline $SrFe_{2.96}Ru_{3.04}O_{11}$ and single-crystal $SrFe_{2.6}Ru_{3.4}O_{11}$ were carried out on the BT7 and BT9 high intensity, triple-axis spectrometers at the NCNR. A pyrolytic graphite PG(002) monochromator and PG(002) analyzer were employed on BT-9 to generate and analyze a λ=2.36 Å neutron beam, and PG filters were used to suppress higher-order wavelength contaminations. Coarse collimations of 40′, 48′, 40′ and 120′ were employed to maximize the intensity. Measurements on BT7 also employed a PG(002) monochromator to generate a λ=2.36 Å neutron beam, and PG filters were used to suppress higher-order wavelength contaminations. BT7 was operated in two-axis (diffraction) mode utilizing a position-sensitive detector.

III. RESULTS AND DISCUSSION

A. Ti-bearing ferrite

Figure 2 shows data for the magnetic susceptibility $\chi = M/H$ for a $BaFe_{3.26}Ti_{2.74}O_{11}$ single crystal in an applied field $\mu_0 H$=0.1 T oriented either parallel or perpendicular to the **c** axis. Two magnetic transitions are indicated by a slow increase in χ with decreasing T below T_1=250 K, and by a maximum at T_2=85 K, and a distinct magnetic anisotropy that indicates an easy **c** axis. The magnetic moment m as a function of $\mu_0 H$ at T=5 K for each field orientation is shown in the inset to Fig. 2, revealing coercive fields $\mu_o H_{c\perp}$=1.0 T and $\mu_o H_{c\|}$=0.75 T for applied fields perpendicular and parallel to the easy **c** axis, respectively. For both field orientations, the rapid increase in $m(H)$ with increasing H at low fields, a linear variation of $m(H)$ for $\mu_o H > 1.2$ T

TABLE II. Atomic coordinates and equivalent isotropic displacement parameters ($Å^2$) for single-crystal $BaFe_{3.26}Ti_{2.74}O_{11}$. U(eq) is defined as one third of the trace of the orthogonalized U_{ij} tensor.

	x	y	z	U(eq)
Ba(1)	1/3	2/3	1/4	0.004(1)
Fe(1)	0	0	0.1450(2)	0.002(1)
Fe(2)	1/2	0	0	0.004(1)
Ti(1)	0	0	0.1450(2)	0.002(1)
Ti(2)	1/2	0	0	0.004(1)
Fe(3)	1/3	2/3	3/4	0.052(2)
O(1)	0.1702(7)	0.3404(1)	0.0808(5)	0.004(1)
O(2)	0.8492(1)	1.6980(2)	1/4	0.004(2)
O(3)	1/3	2/3	0.5783(9)	0.003(2)

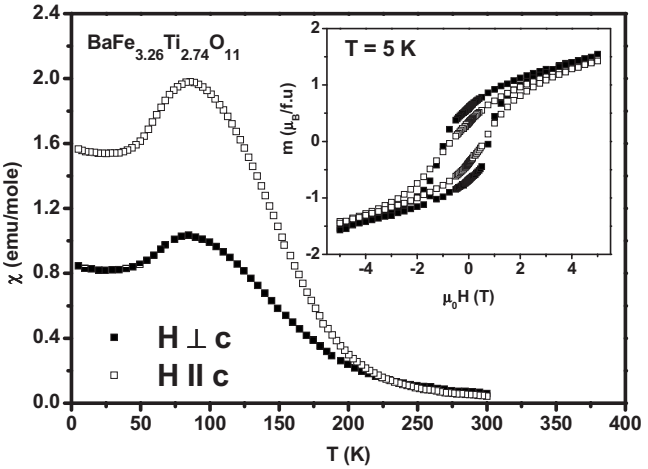

FIG. 2. Temperature dependence of the FC dc magnetic susceptibility $\chi(T) \equiv m(T)/H$ of single-crystal $BaFe_{3.26}Ti_{2.74}O_{11}$ for $\boldsymbol{H} \perp \mathbf{c}$ and $\boldsymbol{H} \| \mathbf{c}$ at applied magnetic field $\mu_o H = 0.1$ T. Inset shows the magnetic moment m vs. H at temperature $T = 5$ K.

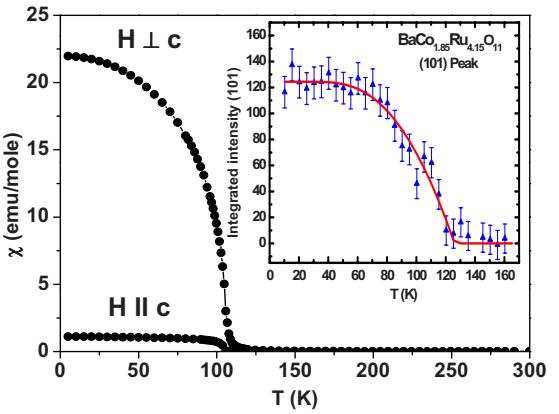

FIG. 4. (Color online) Magnetic susceptibility $\chi(T) \equiv m(T)/H$ of single-crystal $BaCo_{1.8}Ru_{4.2}O_{11}$ for two crystallographic orientations ($\boldsymbol{H} \| \mathbf{c}$ and $\boldsymbol{H} \perp \mathbf{c}$) at applied magnetic field $\mu_o H = 0.1$ T. Inset shows the integrated intensity of the (101) magnetic diffraction peak as a function of temperature T for single-crystal $BaCo_{1.8}Ru_{4.2}O_{11}$. The solid curve is a mean-field fit to the data.

(both above and below T_2), and the failure for $m(H)$ to saturate at high fields are typical of a canted AFM or ferrimagnetic state.[27] Indeed, spin canting out of the **a**-**b** plane may be induced by antisymmetric Dzyaloshinsky-Moriya (DM) interactions[28,29] appropriate for spins in the noncentrosymmetric structure of $BaFe_{3.26}Ti_{2.74}O_{11}$.

Figure 3 shows $m(H)$ for a $BaFe_{3.26}Ti_{2.74}O_{11}$ single crystal at $T = 130$ K, which exhibits a very small coercive field $\mu_o H_{c\perp} = \mu_o H_{c\|} = 4.5 \times 10^{-4}$ T. As shown in the inset, above $T = 250$ K, $m(H)$ exhibits no anisotropy and varies linearly with magnetic field, consistent with paramagnetic behavior. A Curie-Weiss fit to the data over the interval 260 K $< T <$ 360 K yields a Weiss temperature $\theta_W = 220$ K (indicating predominantly FM interactions between spins) and an effective magnetic moment $\mu_{\text{eff}} = 4.73\mu_B$, which is consistent with divalent Fe^{2+}, but is about $1\mu_B$ lower than the value expected for trivalent Fe^{3+}. Single-crystal $BaFe_{3.26}Ti_{2.74}O_{11}$ exhibits an

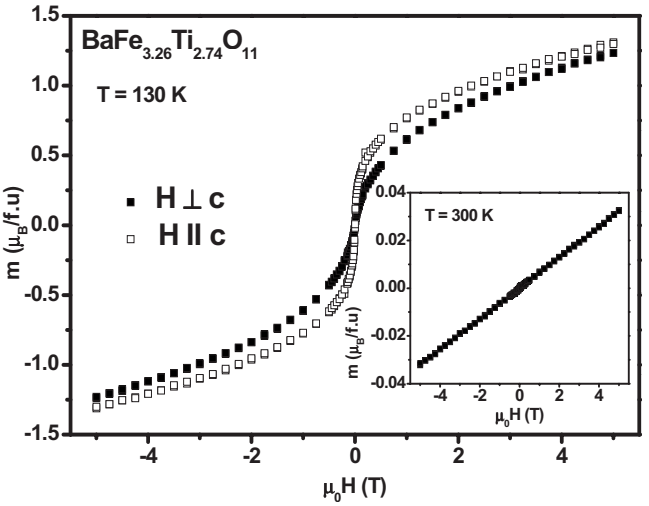

FIG. 3. Magnetic moment m vs. applied magnetic field H at temperature $T = 130$ K for single-crystal $BaFe_{3.26}Ti_{2.74}O_{11}$. Inset shows m vs H at $T = 300$ K.

intermediate value $T_1 \approx 250$ K for the upper magnetic ordering temperature, compared to those ($T_1 \approx 100$ to 500 K) for other *R*-type ferrites based upon Ru. Moreover, the basal-plane electrical resistance of our single-crystal $BaFe_{3.26}Ti_{2.74}O_{11}$ is $R_{300\ \text{K}} \sim 20$ MΩ, which is very high compared to $(\text{Ba,Sr})M_{2\pm x}\text{Ru}_{4\mp x}\text{O}_{11}$ (M=Fe,Co) analogs, and in the range of typical insulators. It is particularly noteworthy that complete replacement of Ru [thought to be

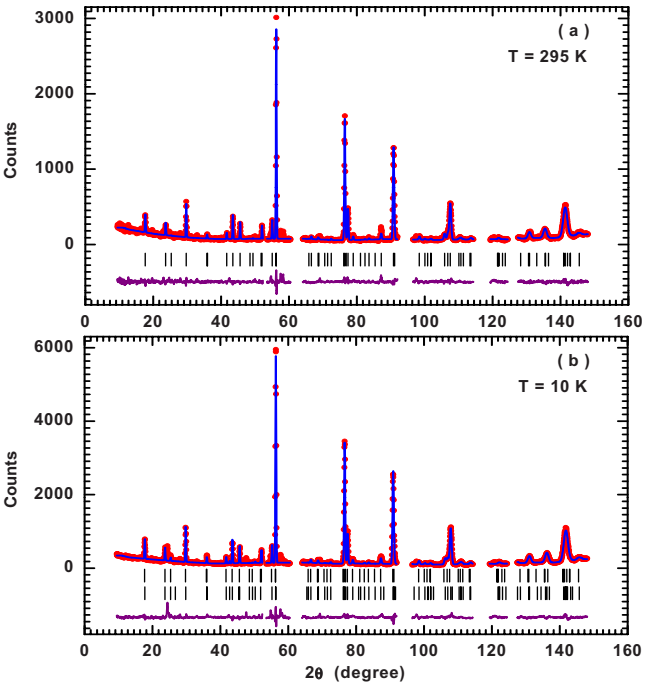

FIG. 5. (Color online) The (a) $T = 295$ K and (b) 10 K diffraction patterns and refinements for $BaCo_{1.68}Ru_{4.32}O_{11}$. Tick marks indicate the positions of Bragg peaks, and the curve at the bottom of each figure indicates the difference between the observed and calculated intensities. Excluded regions correspond to angles corresponding to Bragg peaks arising from the Al sample holder.

TABLE III. Refined structure parameters for polycrystalline $BaCo_{1.68}Ru_{4.32}O_{11}$ at 295 and 10 K. The crystal structure was solved in space group $P6_3/mmc$. The magnetic structure was solved using representational analysis. Atomic positions: Ba:$2c(1/3,2/3,1/4)$, Co/Ru(1):$4e(0,0,z)$, Ru/Co(2):$6g(1/2,0,0)$, Co:$2d(2/3,1/3,1/4)$, O(1):$12k(x,2x,z)$, O(2):$6h(2y,y,1/4)$, and O(3):$4f(2/3,1/3,z)$. A value of 0 for the uncertainty indicates the parameter was not refined.

		295 K	10 K	Magnetic basis vectors
	a (Å)	5.8351(2)	5.8315(1)	
	c (Å)	13.4771(5)	13.4427(5)	
Co/Ru(1)	z	0.1500(5)	0.1512(4)	
	n(Co/Ru)	0.03(2)/0.97(2)	0.03(0)/0.97(0)	
	M_z (μ_B)			(0,0,1)
Co/Ru(2)	n(Co/Ru)	0.21(2)/0.79(2)	0.21(0)/0.79(0)	
	M_x (μ_B)		3.1(2)	(1,2,0), (−1,1,0), (−2,−1,0)
	M_y (μ_B)		6.3(5)	(−1.−2.0), (2,1,0), (0,0,1)
	M_z (μ_B)		0(0)	
	M_{tot} (μ_B)		5.4(4)	
Co	M_z (μ_B)		0.5(2)	(0,0,1)
O(1)	x	0.169(1)	0.1700(9)	
	z	0.0797(4)	0.0788(4)	
O(2)	y	0.1461(7)	0.1469(6)	
O(3)	z	0.4183(7)	0.4189(7)	
	Rp (%)	8.38	8.17	
	wRp (%)	11.7	11.9	
	χ^2	1.75	3.44	
Overall temperature factor		0.83(6)	0.85(5)	

mixed valent $3^+/5^+$ (Ref. 13)] by Ti^{4+} yields a wide-gapped insulator since partial replacement of Ru by Co^{2+} (or possibly Co^{3+}) yields metallic or weakly metallic states and soft FM order well below room temperature,[11–13] and partial replacement of Ru by Fe^{2+} or Fe^{3+} (or possibly mixed valent, $2^+/3^+$) yields narrow-gap semiconductors with magnetic transition temperatures as high as 490 K.[11]

B. Co-bearing ferrites

Previously published $\chi(T)$ data for single-crystal $BaCo_{1.85}Ru_{4.15}O_{11}$ (Ref. 11) in an applied field $\mu_0 H=0.1$ T (either parallel or perpendicular to the **a**-**b** plane) are shown in Fig. 4. It is curious that $\chi(T)$ is strongly anisotropic at low T (being much higher for $\boldsymbol{H}\perp\mathbf{c}$), in spite of the fact that this composition is a very soft ferromagnet (coercive field $\mu_o H_{c\|}=0.0002$ T and $\mu_o H_{c\perp}=0.02$ T at $T=5$ K) with a saturation moment $m_S\approx 1.8\pm 0.1\mu_B$/f.u. at $T=5$ K.[11–13] The inset in Fig. 4 shows the temperature dependence of the integrated magnetic intensity of the (101) neutron diffraction peak for single-crystal $BaCo_{1.85}Ru_{4.15}O_{11}$, as determined from measurements on BT7. The solid curve is a mean-field fit to the data that yields an estimated ordering temperature of $T_C=127(3)$ K, which is in reasonable agreement with our susceptibility and resistivity data.[11]

Room-temperature ($T=295$ K) neutron powder diffraction data taken on BT1 with a neutron wavelength $\lambda=2.079$ Å were used to refine the crystal structure of $BaCo_{1.68}Ru_{4.32}O_{11}$ in the hexagonal space group $P6_3/mmc$. The occupancies of the $M(1)$ and $M(2)$ crystallographic sites were refined assuming a mixed occupancy by Ru and Co cations, yielding the composition $BaCo_{1.68}Ru_{4.32}O_{11}$, which is in reasonable agreement with x-ray diffraction results.[13] Alternative refinements that allowed both Co and Ru to occupy the $M(3)$ site showed that this site remains fully occupied by Co within experimental uncertainties. Diffraction data taken at $T=295$ K and 10 K, along with their refinements, are shown in Figs. 5(a) and 5(b), respectively. Details of the refined parameters are presented in Table III (one standard deviation represents the uncertainty in the neutron scattering data). Comparison of the high- and low-temperature data indicates that at least one magnetic impurity phase is present, but the small magnitude of the impurity peaks and the low value of the goodness of fit parameter ($\chi^2=1.75$) for the refinement to the $T=295$ K data indicate that the impurity phase comprises no more than a few per cent of the sample.

Representational analysis was carried out to determine the allowed irreducible representations (i.e., a group representation whose dimension cannot be reduced by similarity transform, and which determines the possible basis vectors that describe the magnetic symmetry group and magnetic diffracted intensities) for the magnetic structure, assuming spins on the $M(1)$, $M(2)$, and $M(3)$ sites. The Γ_3 and Γ_9 representations were found to be the only ones simultaneously allowed for all three sites. Refinements of the $T=10$ K data using each representation in turn and the occupancies of the z and $M(2)$ sites determined from the $T=295$ K data, led us

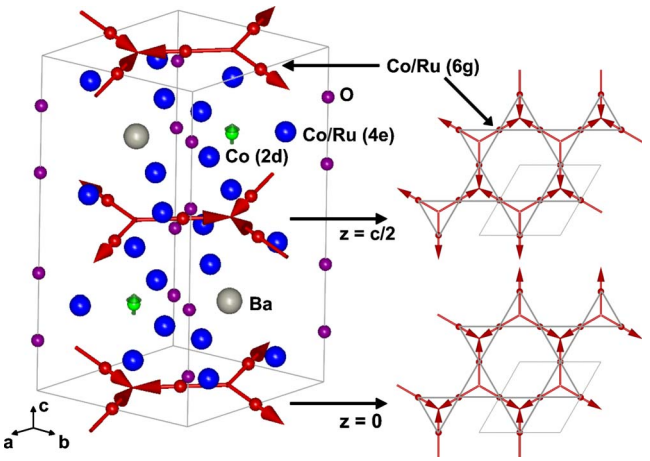

FIG. 6. (Color online) Magnetic order in $BaCo_{1.68}Ru_{4.32}O_{11}$, assuming Co fully occupies the 6*g* and 2*d* lattice sites. Atoms on the 6*g* [*M*(2)] site form a kagome sublattice in the **a**-**b** plane, consisting of corner sharing triangles. Spins forming the triangles are oriented at 120° to one another and form an antiferromagnetically ordered state in which they alternate between pointing all into, or all out, of each triangle. Spins on the 2*d* [*M*(3)] site are ferromagnetically ordered along the **c** axis. The moment on the 4*e* [*M*(1)] site is assumed to be 0.

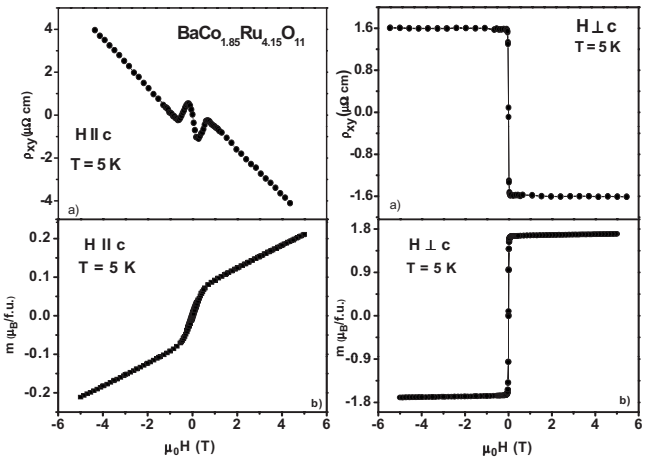

FIG. 7. Left panel: (a) transverse resistivity ρ_{xy} and (b) magnetic moment versus magnetic field $\boldsymbol{H}\|\mathbf{c}$ for single-crystal $BaCo_{1.8}Ru_{4.2}O_{11}$ at temperature $T=5$ K. Right panel: (a) transverse resistivity ρ_{xy} and (b) magnetic moment versus magnetic field $\boldsymbol{H}\perp\mathbf{c}$ at $T=5$ K. The current is in **ab** plane.

to conclude that the Γ_3 representation gave the best fit to the data. We found that only a small moment (with a value comparable to its uncertainty) exists for Co on the $M(1)$ site, which is reasonable given that the $M(1)$ site occupancy is 97% (nonmagnetic) Ru and only 3% Co. Due to the low Co occupancy of this site, we therefore repeated the refinement assuming that the $M(1)$ site is nonmagnetic. As shown in Table III, the final refinement resulted in a moment per spin of $m=5.4(4)\mu_B$ for the $M(2)$ site (which is reasonable for a high-spin $S=2$, Co^{3+} ion), and we find $m=0.5(2)\mu_B$ for Co (e.g., low-spin, mixed-valent Co^{+3}/Co^{+2}) moments on the $M(3)$ site.

As stated above, antiferromagnetically correlated transition element spins occupying the $M(2)$ sites within the kagome layers can experience magnetic frustration. In accordance with the Γ_3 representation, the *average* magnetic order is the so-called "all-in, all-out," 120° AFM state in which three spins occupying the corners of the triangular unit of successive kagome layers alternately point all toward, or all away from, the center of each corner-sharing triangle, as shown in Fig. 6. Spins on the $M(3)$ sites undergo weak FM order along the **c**-axis. It is important to emphasize that this is the *average magnetic structure* determined from the refinements, and that only 21% of the $M(2)$ sites are occupied by Co. Hence, it is unlikely that there is a contiguous all-in, all-out structure over the whole sample. Nevertheless, the Γ_3 representation permits canting of the $M(2)$ spins out of the kagome plane along the **c** direction, which would break chiral symmetry, if a contiguous all-in, all-out structure were to exist on the kagome sublattice. Due to the limited number of magnetic reflections, we are unable to reliably refine a **c**-axis component to the moment of these spins. On the other hand, the goodness-of-fit indicators for refinements that include a small spin canting are the same as for refinements that do not include canting. Furthermore, a canted state for the $M(2)$ spins and the weak FM order among the $M(3)$ sites would be consistent with the overall FM interactions determined from our magnetization data, and with a previous report[14] of a canted spin structure for isostructural $BaMn_2Ru_4O_{11}$, which is a rare example of nonzero spin chirality within an ordered state.[23] As we discuss next, our Hall measurements also point to a canted spin arrangement on the $M(2)$ sites.

Data for the transverse magnetoresistivity ρ_{xy} at $T=5$ K for single-crystal $BaCo_{1.85}Ru_{4.15}O_{11}$ are shown in Fig. 7. The transverse magnetoresistivity is traditionally expressed in the following form for ferromagnets:

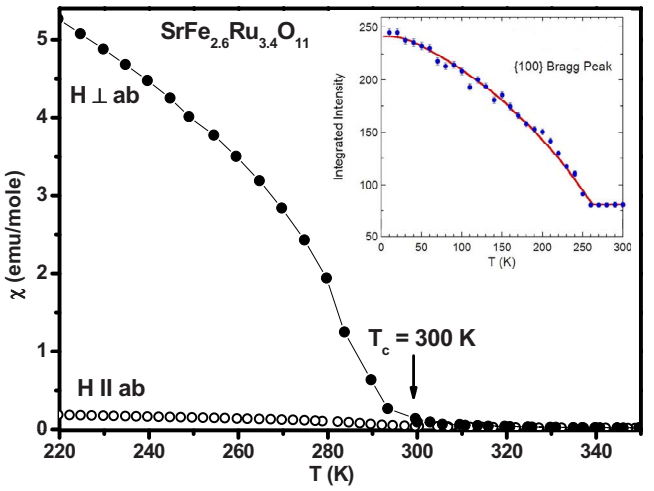

FIG. 8. (Color online) Temperature dependence of the FC magnetic susceptibility $\chi(T)\equiv m(T)/H$ of single-crystal $SrFe_{2.6}Ru_{3.4}O_{11}$ for $\boldsymbol{H}\perp\mathbf{c}$ and $\boldsymbol{H}\|\mathbf{c}$ at applied magnetic field $\mu_o H=0.1$ T. Inset shows the integrated intensity (proportional to the square of the ordered moment) of the magnetic (100) peak as a function of temperature. The solid curve is a power law fit to the data with a $T_C=262(1)$ K and $2\beta=0.45(1)$.

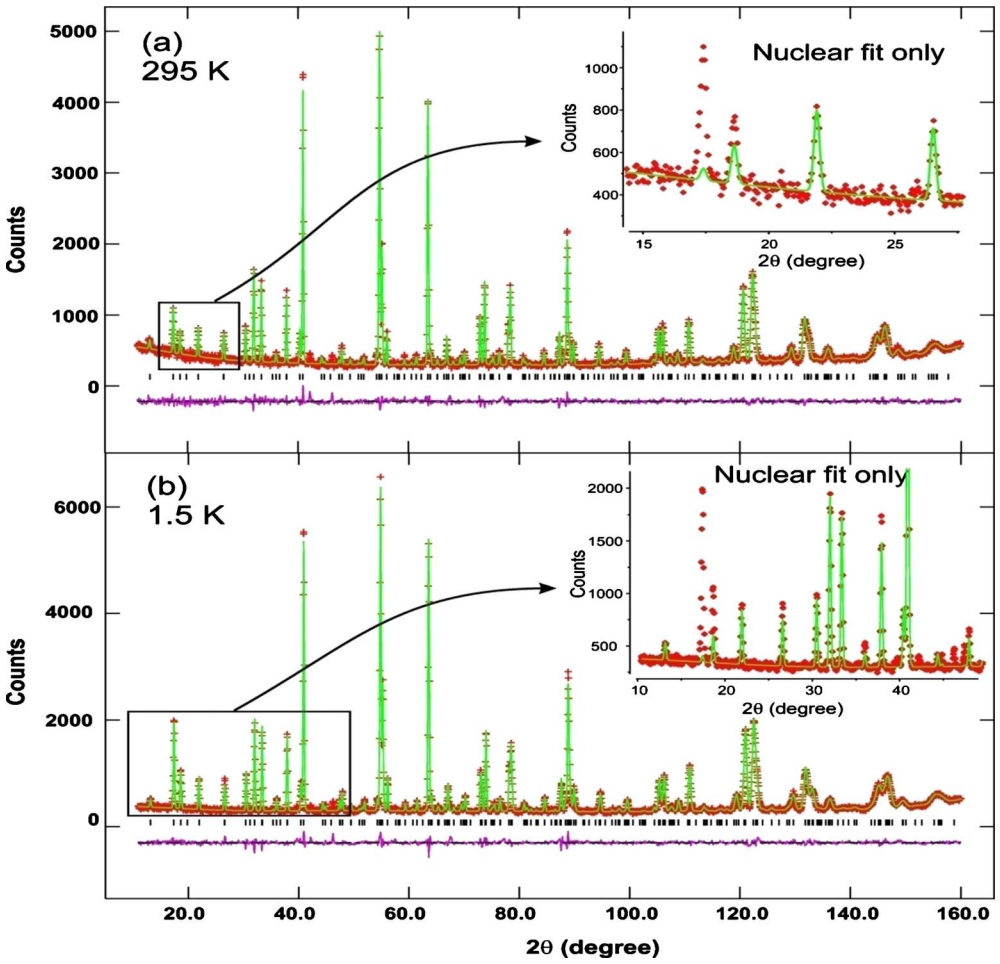

FIG. 9. (Color online) Neutron diffraction patterns and their refinements for $T=295$ K and 1.5 K for polycrystalline $SrFe_{2.96}Ru_{3.04}O_{11}$. The insets show the fit using only the structural component of the scattering, which indicates that the sample retains some magnetic order at room temperature. Tick marks indicate the positions of Bragg peaks, and the curve at the bottom of each figure indicates the difference between the observed and calculated intensities.

$$\rho_{xy} = R_0 \mu_0 H + 4\pi M R_s, \tag{1}$$

where R_0 is the Hall coefficient resulting from the Lorentz force on the carriers, and R_s is the anomalous Hall coefficient, whose origin is attributed to the magnetization $M(H)$ and spin-orbit coupling.[30,31] Clearly, ρ_H is expected to have a field dependence similar to that of the magnetization in ferromagnets below T_C,[30] which is indeed the behavior observed for ρ_{xy} and $m(H)$ data for $BaCo_{1.85}Ru_{4.15}O_{11}$ for $\boldsymbol{H} \perp \mathbf{c}$ axis, as shown in Fig. 7(b) (right panel). However, an unusual, non-monotonic field dependence of ρ_{xy} with magnetic field $\boldsymbol{H} \| \mathbf{c}$ axis and current $\boldsymbol{J} \perp \mathbf{c}$ axis is observed for $\mu_o|H| < 0.6$ T, with sharp peaks occurring at $\mu_o H = \pm 0.15$ T, as shown in Fig. 7(a) (left panel). The monotonic behavior of the moment $m(H)$ in the field range $\mu_o|H| < 0.6$ T contrasts with the non-monotonic behavior seen in our ρ_{xy} data [Fig. 7(b), left panel] and is therefore in conflict with the usual description of the anomalous Hall effect (AHE) given in Eq. (1), and a new mechanism is required to explain it.

A nonmonotonic ρ_{xy} may result[16] from noncoplanar spin textures of nonzero scalar spin chirality $K_S \equiv \boldsymbol{S}_1 \cdot (\boldsymbol{S}_2 \times \boldsymbol{S}_3)$, which is proportional to the solid angle subtended by the neighboring spins $\boldsymbol{S}_i$(i=1–3) residing on a kagome triangle, and acts as a gauge flux for charge carriers moving in the background of atomic spins.[22] Note that our magnetic neutron diffraction results for $BaCo_{1.68}Ru_{4.32}O_{11}$ do not rule out a small, nonzero K_S for the Co spins on the $M(2)$ sites. In the case of the current/field configuration $\boldsymbol{J} \perp \boldsymbol{H} \| \mathbf{c}$, the transverse motion of carriers depends on the sum of the Lorentz contribution, the AHE of the **c**-axis magnetization on the $M(2)$ and $M(3)$ sites, and the THE contribution of the nonzero scalar chirality of the $M(2)$ sublattice. The Lorentz and spin-orbit contributions to the AHE are normally expected to be *monotonic* functions of the applied field. Therefore, we propose the following explanation for our $BaCo_{1.68}Ru_{4.32}O_{11}$ ρ_{xy} data in terms of a *nonmonotonic* THE arising from nonzero spin chirality: For $\boldsymbol{H} \| \mathbf{c}$ and $\mu_o|H| < 0.15$ T, the canting angle of the $M(2)$ spins initially increases with field, causing K_S to increase and consequently, the magnitude of the THE to increase. The strong decrease of $|\rho_{xy}|$ for 0.15 T $< \mu_o|H| < 0.6$ T indicates that the K_S of the $M(2)$ spins abruptly decreases since it probably results from a relatively strong contribution of the THE generated by a spin rearrangement along the **c** axis, as recently suggested by Hall data for a Mn-bearing *R*-type ferrite.[32] However, further spin alignment

TABLE IV. Refined structure parameters for polycrystalline $SrFe_{2.96}Ru_{3.04}O_{11}$ at 295 and 1.5 K. The crystal space group is $P6_3/mmc$ and the magnetic space group is $P6_3/mm'c'$. Atomic positions: Sr:$2c(1/3,2/3,1/4)$, Fe/Ru(1):$4e(0,0,z)$, Ru/Fe(2):$6g(1/2,0,0)$, Fe:$2d(2/3,1/3,1/4)$, O(1):$12k(x,2x,z)$, O(2):$6h(x,2x,1/4)$, and O(3):$4f(1/3,2/3,z)$.

		295 K	1.5 K
	a (Å)	5.8465(1)	5.8421(1)
	c (Å)	13.3803(3)	13.3439(3)
Fe/Ru(1)	z	0.1476(3)	0.1475(2)
	n(Fe/Ru)	0.59(5)/0.41(5)	0.59/0.41(4)
	M_z (μ_B)	1.8(1)	2.4(1)
Fe/Ru(2)	n(Fe/Ru)	0.26(3)/0.74(3)	0.26/0.74(3)
	M_z (μ_B)	−0.9(2)	−1.3(1)
Fe	M_z (μ_B)	−2.8(2)	−3.6(2)
O(1)	x	0.1723(4)	0.1724(3)
	z	0.0830(2)	0.0828(2)
O(2)	x	−0.1522(4)	−0.1516(3)
O(3)	z	0.5861(6)	0.5855(4)
	Rp (%)	3.99	4.24
	wRp (%)	5.06	5.57
	χ^2	1.215	1.504

Anisotropic temperature factors $U_{ij}\times 100$ (Å^2) at 295 K (first line) and 1.5 K (second line).

	B_{11} (Å^2)	B_{22} (Å^2)	B_{33} (Å^2)	B_{12} (Å^2)	B_{13} (Å^2)	B_{23} (Å^2)
Sr	1.0(2)	1.0(2)	2.6(4)	0.5(9)	0	0
0.8(1)	0.8(1)	0.9(3)	0.40(7)	0	0	
Fe/Ru(1)	0.4(1)	0.4(1)	2.0(2)	0.19(5)	0	0
	0.36(9)	0.36(9)	1.0(1)	0.18(4)	0	0
Fe/Ru(2)	0.7(1)	2.1(2)	0.74(8)	1.0(2)	−0.1(1)	−0.2(2)
	0.90(9)	2.5(2)	0.5(1)	1.27(8)	0.6(4)	1.0(7)
Fe	0.6(1)	0.6(1)	5.3(3)	0.32(7)	0	0
	0.8(1)	0.8(1)	3.8(3)	0.39(7)	0	0
O(1)	1.2(1)	0.8(1)	1.2(1)	0.41(7)	0.47(6)	0.9(1)
	1.00(8)	0.6(1)	1.0(1)	0.31(6)	0.38(4)	0.75(8)
O(1)	0.4(2)	1.7(2)	1.8(2)	0.2(1)	0	0
	0.1(2)	1.3(1)	1.1(2)	0.05(8)	0	0
O(3)	1.5(2)	1.5(2)	2.2(4)	0.76(8)	0	0
	1.8(1)	1.8(1)	0.8(3)	0.90(7)	0	0

along the **c** axis with additional increases of $\boldsymbol{H}\|\mathbf{c}$ is inhibited since the **c** axis is the *hard axis* for Co-bearing ferrites, in contrast to the Mn analog, where the **c** axis is an *easy axis*. The maximum applied magnetic field is 5 T, which is expected to be much lower than typical exchange fields in FM materials with $T_C \approx 10^2$ K. Therefore, K_S does not vary appreciably for $0.6\ \mathrm{T} < \mu_o|H| < 5$ T, and ρ_{xy} is monotonic and follows the linear dependences of the magnetization [Fig. 7(b), left panel] of the $M(2)$ and $M(3)$ sites and the Lorentz force, consistent with the usual AHE predicted by Eq. (1).

We now return to the monotonic behavior of $\rho_{xy}(T=5\ \mathrm{K}, H)$ for single-crystal $BaCo_{1.85}Ru_{4.15}O_{11}$ shown in Fig. 7 (right panel) and obtained with $\boldsymbol{J}\|\boldsymbol{H}\perp\mathbf{c}$ axis. We emphasize that in this nonstandard configuration, the transverse motion of carriers will not arise from a Lorentz force but will depend mainly on the magnetization and a weak contribution from the dipolar magnetic field generated by the Co moments on the $M(3)$ and $M(2)$ sites. Indeed, a monotonic field dependence of ρ_{xy} is observed as it is expected according to Eq. (1) [Fig. 7(b), right panel]. The negative slope of $\rho_{xy}(H)$ in the saturation regime of $m(H)$ indicates that the dominant charge carriers are electrons. Note that there is an approximate *threefold increase* in $\rho_{xy}(\mu_0 H=-5\ \mathrm{T}, T=5\ \mathrm{K})$ for $\boldsymbol{H}\|\mathbf{c}$ axis, compared to that for $\boldsymbol{H}\perp\mathbf{c}$ axis; this observation confirms our assumption that the THE is the major contributor to ρ_{xy} at low fields, including fields applied in the hard direction. Similar observations in geometrically frustrated systems with spin canting,[20,21] and in isostructural

$BaMn_{2.49}Ru_{3.51}O_{11}$,[32] suggest that $BaCo_{2\pm x}Ru_{4\mp x}O_{11}$ is a good candidate to test the validity of the spin chirality mechanism for the THE.

C. Fe-bearing ferrite

Single-crystal $SrFe_{2.6}Ru_{3.4}O_{11}$ is known to exhibit long-range magnetic order below $T_C=300$ K.[11] Magnetization data at $\mu_o H=0.1$ T (see Fig. 8) reveal a strong magnetic anisotropy of $\chi(H_{\perp ab})/\chi(H_{\parallel ab}) \approx 300$ for $SrFe_{2.6}Ru_{3.4}O_{11}$ at $T=5$ K, indicating an easy axis parallel to the **c** direction.[11] Apparently, interchanging Fe for Co in *R*-type ferrites rotates the magnetic easy axis by 90°. The inset to Fig. 8 shows the integrated intensity of the (100) Bragg peak as a function of temperature, as determined from neutron scattering measurements performed on BT9. The temperature dependence of the integrated intensity is in good agreement with our susceptibility data, and the solid curve is a power-law fit that yields an estimated ordering temperature of $T_C=262(1)$ K. We note that it is unusual for a power-law to fit data over the entire temperature range of the ordered state, but such behavior has been seen in low-dimensional systems such as the layered cuprate Sm_2CuO_4.[33] A mean-field fit yields systematic deviations from the data and a substantially poorer fit quality.

Nuclear and magnetic neutron powder diffraction data were taken on polycrystalline $SrFe_{2.96}Ru_{3.04}O_{11}$ on BT1 using a $\lambda=1.540$ Å neutron beam. The resulting refinements for $T=295$ and 1.5 K, which have respective goodness of fit values of $\chi^2=1.215$ and 1.504, are shown in Figs. 9(a) and 9(b), respectively. We list the values of parameters determined from the refinements in Table IV. The insets to Fig. 9 show low-angle diffraction data at both temperatures and the nuclear refinement. From the insets, it is obvious that the nuclear refinement does not account for all the Bragg peaks at lower scattering angles at both temperatures measured. The discrepancy is most obvious for the (100) peak ($2\theta=17.5°$), which suggests the sample undergoes another magnetic transition above $T=295$ K. In order to determine if a higher temperature magnetic transition does occur, we measured the temperature dependence of the (100) Bragg peak of polycrystalline $SrFe_{2.96}Ru_{3.04}O_{11}$ up to $T=500$ K on BT9. The results are shown in Fig. 10, in which we see that the integrated intensity of the (100) peak increases with decreasing temperature below $T \approx 400$ K. A mean-field fit to the data yields an ordering temperature of $T_C=403(4)$ K. Looking at Fig. 9(a), the background at low angles gently decreases with increasing 2θ, while in Fig. 9(b) this background is absent. This behavior is consistent with a paramagnetic contribution to the scattering at $T=295$ K. Thus, the transition at $T_C=403(4)$ K may not involve all of the spins, and that the sample may only partially order at this temperature. At $T=1.5$ K, all spins lie along the **c** axis in a collinear structure, with spins on equivalent crystallographic sites ferromagnetically aligned as shown in Fig. 11. Spins on the $M(2)$ and $M(3)$ sites are ferromagnetically aligned with respect to each other, but are antiferromagnetically aligned with respect to the spins on the $M(1)$ sites.

The $m(H)$ [Fig. 12(a)] and ρ_{xy} [Fig. 12(b)] data for single-crystal $SrFe_{2.6}Ru_{3.4}O_{11}$ at $T=280$ K and $\boldsymbol{H}\|\mathbf{c}$ are distinctly different from the Co-based ferrite, as is apparent in Fig. 12(b): ρ_H has a large field dependence for $\mu_o H \ll 1.0$ T and $T \leq T_c$ and increases with increasing field, similar to the field dependence of the magnetization [Fig. 12(a)], which is typical of the AHE for FM materials with spin-orbit coupling. This behavior is also consistent with the collinear magnetic structure determined from our powder diffraction measurements on $SrFe_{2.96}Ru_{3.04}O_{11}$, which would demand $K_S=0$, and no THE contributions to ρ_H.

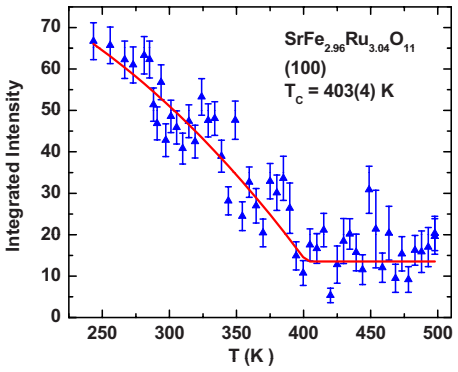

FIG. 10. (Color online) The integrated intensity of the (100) Bragg peak at high temperatures determined from high-temperature neutron scattering measurements. The line is a mean-field fit to the data, yielding a magnetic transition temperature $T_C=403(4)$ K.

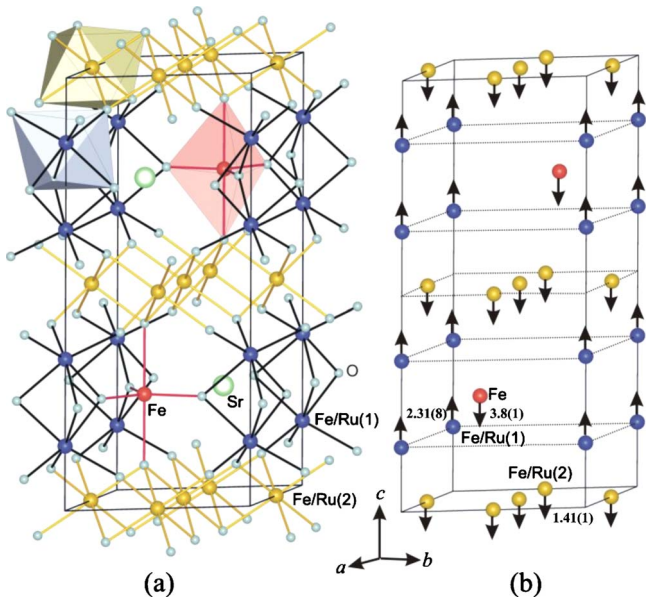

FIG. 11. (Color online) (a) The nuclear structure for polycrystalline $SrFe_{2.96}Ru_{3.04}O_{11}$ determined from refinements to neutron diffraction data taken at $T=295$ K. (b) The magnetic order of $SrFe_{3.26}Ru_{2.74}O_{11}$ at $T=1.5$ K determined from refinements to neutron diffraction data. Spins lie along the **c**-axis, with spins on equivalent crystallographic sites possessing FM order. Spins on the 6*g* (yellow spheres) and 2*d* (red spheres) sites are ferromagnetically ordered, while spins on the 4*e* sites (blue spheres) are antiferromagnetically ordered with respect to the spins on both the 6*g* and 2*d* sites.

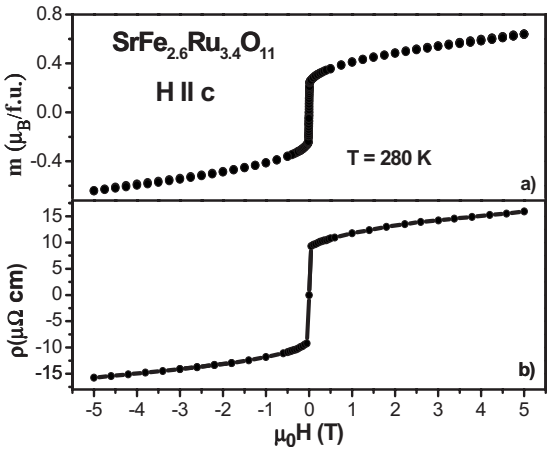

FIG. 12. (a) Field dependence of the magnetic moment of $SrFe_{2.6}Ru_{3.4}O_{11}$ single crystal at $T=280$ K. (b) Magnetic field dependence of the Hall resistivity ρ_{xy} of a $SrFe_{2.6}Ru_{3.4}O_{11}$ single crystal at 280 K. Current is in the **ab** plane.

IV. SUMMARY AND CONCLUSIONS

Variations of the 3*d*-element content in the *R*-type ferrites have a profound effect on their magnetic and electrical properties. Complete substitution of Fe^{2+} ($3d^6$ electronic configuration) by Co^{2+}/Co^{3+} ($3d^7/3d^6$ electronic configuration) in $(Ba,Sr)M_{2\pm x}Ru_{4\mp x}O_{11}$ (M=Fe,Co) ferrites leads to an evolution of the easy direction away from the hexagonal **c** axis for semiconducting/high-T_C, Fe-bearing compositions, to approximate alignment within the **ab**-plane for metallic/low-T_C, Co-bearing compositions. The differences in electron transport between 3*d*-only and 3*d*/4*d*-containing ferrites might be attributed to the stronger hybridization of either Co or Fe with mixed-valent Ru^{3+}/Ru^{5+} ($4d^5/4d^3$) states via superexchange through the oxygen O^{2-} 2*p* orbitals. This should lead to a wider conduction band relative to the Fe/Ti ferrites.

Specific conclusions drawn from our neutron diffraction and magnetotransport studies are as follows:

(1) The magnetic structure of polycrystalline $SrFe_{2.96}Ru_{3.04}O_{11}$ ($T_C \approx 300$ K) deduced from neutron diffraction is ferrimagnetic, collinear at $T=5$ K. The measured ρ_{xy} for single-crystal $SrFe_{2.6}Ru_{3.4}O_{11}$ for $\boldsymbol{H}\|\mathbf{c}$ is found to correspond very closely to the magnetization data, which gives no indication of nonzero scalar spin chirality.

(2) Neutron powder refinements for $BaCo_{1.68}Ru_{4.32}O_{11}$ revealed a noncollinear, all-in/all-out structure.[14] The powder refinements are consistent with a collinear, **c**-axis moment on the $M(3)$ sites, and possible canting out of the kagome plane of magnetic moments on $M(2)$ sites, which is expected to generate nonzero scalar spin chirality. The unusual nonmonotonic field dependence of the AHE observed in single-crystal $BaCo_{1.85}Ru_{4.15}O_{11}$ for $\boldsymbol{H}\|\mathbf{c}$ is interpreted as further, strong evidence of nonzero scalar spin chirality that drives a THE.

(3) Magnetic measurements on single-crystal $BaFe_{3.26}Ti_{2.74}O_{11}$ reveal distinct magnetic transitions at $T_1=250$ K and $T_2=85$ K. The temperature- and field-dependent magnetic anisotropies suggest that DM interactions and competing nearest- and next-nearest-neighbor interactions contribute to the complex magnetic order for $BaFe_{3.26}Ti_{2.74}O_{11}$. Detailed studies of the magnetic structure of $BaFe_{3.26}Ti_{2.74}O_{11}$, as for other representatives of the *R*-type ferrites, would be highly desirable.

ACKNOWLEDGMENTS

Research at the University of Kentucky was supported by U.S. DOE under Grant No. DOE-FG∅2-97ER45653. B.G.U. acknowledges support from the NIST/NRC Postdoctoral Research Associateship Program.

*Corresponding author. Department of Physics and Astronomy, University of Kentucky, Lexington, KY 40506-0055, USA; lshlyk@gmail.com

[1] D. Grundler, Phys. World **15**, 39 (2002).
[2] D. D. Awschalom, M. E. Flatté, and N. Samarth, Sci. Am. **286**, 66 (2002).
[3] I. Žutić, J. Fabian, and S. Das Sarma, Rev. Mod. Phys. **76**, 323 (2004).
[4] D. D. Awschalom and M. E. Flatté, Nat. Phys. **3**, 153 (2007).
[5] W. E. Pickett and J. S. Moodera, Phys. Today **54**, 39 (2001).
[6] X. Zou and G. Xiao, Appl. Phys. Lett. **91**, 113512 (2007).
[7] K. Balakrishnan, S. K. Arora, and I. V. Shvets, J. Phys.: Condens. Matter **16**, 5387 (2004).
[8] W. L. Zhou, K.-Y. Wang, C. J. O'Connor, and J. Tang, J. Appl. Phys. **89**, 7398 (2001).
[9] T. Dietl, J. Appl. Phys. **103**, 07D111 (2008).
[10] T. Hynninen, H. Raebiger, J. von Boehm, and A. Ayuela, Appl. Phys. Lett. **88**, 122501 (2006).
[11] L. Shlyk, S. Kryukov, B. Schüpp-Niewa, R. Niewa, and L. E. De Long, Adv. Mater. (Weinheim, Ger.) **20**, 1315 (2008).
[12] L. Shlyk, S. Kryukov, B. Schüpp-Niewa, R. Niewa, and L. E. De Long, J. Appl. Phys. **103**, 07D112 (2008).
[13] B. Schüpp-Niewa, L. Shlyk, S. Kryukov, L. E. De Long, and R. Niewa, Z. Naturforsch. B **62**, 753 (2007).
[14] M. L. Foo, Q. Huang, J. W. Lynn, Wei-Li Lee, T. Klimczuk, I. S. Hagemann, N. P. Ong, and R. J. Cava, J. Solid State Chem. **179**, 563 (2006).
[15] M. C. Cadee and D. J. W. Ijdo, J. Solid State Chem. **52**, 302 (1984).
[16] N. Nagaosa, J. Phys. Soc. Jpn. **75**, 042001 (2006).
[17] K. Hida, J. Phys. Soc. Jpn. **70**, 3673 (2001).
[18] X. G. Wen, F. Wilczek, and A. Zee, Phys. Rev. B **39**, 11413 (1989).
[19] T. Kimura, Annu. Rev. Mater. Res. **37**, 387 (2007).
[20] Y. Taguchi, Y. Oohara, H. Yoshizawa, N. Nagaosa, and Y. Tokura, Science **291**, 2573 (2001).
[21] K. Ohgushi, S. Murakami, and N. Nagaosa, Phys. Rev. B **62**, R6065 (2000).
[22] J. Ye, Y. B. Kim, A. J. Millis, B. I. Shraiman, P. Majumdar, and Z. Tesanovic, Phys. Rev. Lett. **83**, 3737 (1999).
[23] D. Grohol, K. Matan, J.-H. Cho, S.-H. Lee, J. W. Lynn, D. G. Nocera, and Y. S. Lee, Nat. Mater. **4**, 323 (2005).

[24] A. C. Larson and R. B. Von Dreele, Los Alamos National Laboratory Report No. LAUR 86-748, 2004 (unpublished).
[25] J. Rodríguez-Carvajal, Physica B **192**, 55 (1993).
[26] A. S. Wills, Physica B **276-278**, 680 (2000).
[27] R. L. Carlin, *Magnetochemistry* (Springer-Verlag, Berlin, 1986).
[28] I. Dzyaloshinsky, J. Phys. Chem. Solids **4**, 241 (1958).
[29] T. Moriya, Phys. Rev. **120**, 91 (1960).
[30] R. Karplus and J. M. Luttinger, Phys. Rev. **95**, 1154 (1954).
[31] L. Berger, Phys. Rev. B **2**, 4559 (1970).
[32] L. Shlyk, S. Parkin, and L. E. De Long, Phys. Rev. B **81**, 014413 (2010).
[33] S. Skanthakumar, J. W. Lynn, J. L. Peng, and Z. Y. Li, J. Appl. Phys. **69**, 4866 (1991).